Stokes-Einstein-like relation for athermal systems and glasses under shear

Daniel J. Lacks
Department of Chemical Engineering, Tulane University, New Orleans, Louisiana 70118
(Received 30 May 2002; published 13 November 2002)

Finite temperature and athermal simulations are used to determine the viscosity μ and diffusivity D for systems undergoing shear flow at shear rate γ and temperature T. Athermal simulations show that $\mu \sim \gamma^{-1}$ and $D \sim \gamma$ due to strain-activated relaxations, leading to an athermal Stokes-Einstein-like relation $\mu D = C_{\mathrm{ASE}}$. Finite temperature simulations show that at high T the Stokes-Einstein relation $\mu D = C_{\mathrm{SE}} T$ is followed, and as T decreases μD diverges in the Newtonian limit, but μD reaches the constant value C_{ASE} for finite γ. These different behaviors of μD suggest that particle dynamics are fundamentally different as jamming is approached by reducing a driving force as opposed to cooling, and that dynamic heterogeneities play a different role in shear-induced dynamics.

DOI: 10.1103/PhysRevE.66.051202 PACS number(s): 66.20.+d, 64.70.Pf

The relationship between the dynamics in thermal systems (atomic and colloidal systems) and athermal systems (e.g., granular materials and foams) is an area of intense recent study [1]. The dynamics in athermal systems are generated by applied driving forces, while the dynamics in thermal systems can be generated by both driving forces and thermal energy. When the driving force or temperature is reduced, both thermal and athermal systems undergo jamming transitions, which are characterized by the cessation of flow. Unresolved questions include how the properties of the unjammed system change as the jamming transition is approached, and the nature of the relationship between jamming due to temperature decrease and jamming due to driving force decrease. The present paper addresses these questions using nonequilibrium molecular dynamics simulations, and an analysis of the potential energy landscape [2].

The system examined is the binary (80–20 %) mixture of Lennard-Jones atoms that prevents crystallization [3]. The Lennard-Jones parameters are ε_{ij} and σ_{ij} for interactions between atoms of type i and type j, where $\varepsilon_{22}=0.5\varepsilon_{11}$, $\sigma_{22}=0.88\sigma_{11}$, $\varepsilon_{12}=1.5\varepsilon_{11}$, and $\sigma_{12}=0.8\sigma_{11}$; the interactions are truncated at the distance of $2.5\sigma_{ij}$ (and shifted with respect to energy, such that the energy is continuous). All of the atoms have the mass m. The following units are used throughout the paper: ε_{11} for energy, σ_{11} for length, ε_{11}/k_B for temperature, $(m\sigma_{11}^2/\varepsilon_{11})^{1/2}$ for time, $\varepsilon_{11}/\sigma_{11}^3$ for stress, $(m\varepsilon_{11}/\sigma_{11}^4)^{1/2}$ for viscosity, and $(\sigma_{11}^2\varepsilon_{11}/m)^{1/2}$ for diffusivity. The simulations are carried out for $N=500$ atoms at the density $\rho=1.2$. The viscosity μ is obtained as

$$\mu = \frac{\langle \tau \rangle}{\gamma}, \tag{1}$$

where $\langle \cdots \rangle$ represents an average over the simulation trajectory and the shear stress τ is calculated as

$$\tau = \left(\frac{1}{V}\right)\left(m\sum_{i=1}^{N} v_{xi}v_{yi} + \sum_{i=1}^{N}\sum_{j=i+1}^{N} r_{ij}f_{ij}\frac{\partial r_{ij}}{\partial x_i}\frac{\partial r_{ij}}{\partial y_j}\right), \tag{2}$$

where V is the volume, v_{xi} and v_{yi} are components of the velocity of particle i, and r_{ij} and f_{ij} are the distance and force between particles i and j (in the athermal simulations described below the velocities are zero). The diffusion constants in the directions perpendicular to flow, D_{yy} and D_{zz}, are obtained from the Einstein equations,

$$D_{yy} = \left(\frac{1}{2}\right)\frac{\langle (\Delta y)^2 \rangle}{t}, \quad D_{zz} = \left(\frac{1}{2}\right)\frac{\langle (\Delta z)^2 \rangle}{t}, \tag{3}$$

where $(\Delta y)^2$ and $(\Delta z)^2$ are the mean-squared displacements relative to initial configurations, and t is the time. The average diffusivity in the directions perpendicular to flow is obtained as $D=(D_{yy}+D_{zz})/2$.

Two types of simulations are carried out.

(1) Nonequilibrium molecular dynamics (NEMD) simulations based on the sllod equations of motion with Lees-Edwards boundary conditions and a Gaussian thermostat [4]. The simulations are run for $(1-10)\times 10^6$ NEMD steps with a time step of 0.01. These simulations are used to determine properties at temperature T and shear rate γ.

(2) Athermal simulations in which the shear strain λ is incremented in very small steps, with energy minimizations carried out after each step. The strain is increased in steps of 0.0001, and these simulations begin from instantaneous configurations during the NEMD trajectory. These athermal simulations correspond to the NEMD simulations in the limits of zero temperature and zero shear rate.

The NEMD results for the viscosity and (inverse) diffusivity as a function of temperature are shown in Fig. 1, both for the $\gamma \to 0$ (Newtonian) limit and for $\gamma=0.001$; for $T>0.6$, the $\gamma=0.001$ results coincide with the $\gamma \to 0$ results to within the errors of the simulation. As expected, the viscosity and inverse diffusivity increase as the temperature decreases. Previous studies on the same system have shown that in the $\gamma \to 0$ limit the viscosity [5] and inverse diffusivity [3] diverge as $\mu \sim (T-T_c)^{-2.45}$ and $1/D \sim (T-T_c)^{-2.00}$, respectively, where $T_c=0.435$ is the mode coupling crossover temperature. These functional forms for μ and $1/D$ are included in Fig. 1, which shows that the present $\gamma \to 0$ results agree with these previous results (these functional forms are relevant only near T_c, and are not expected to apply far from T_c).

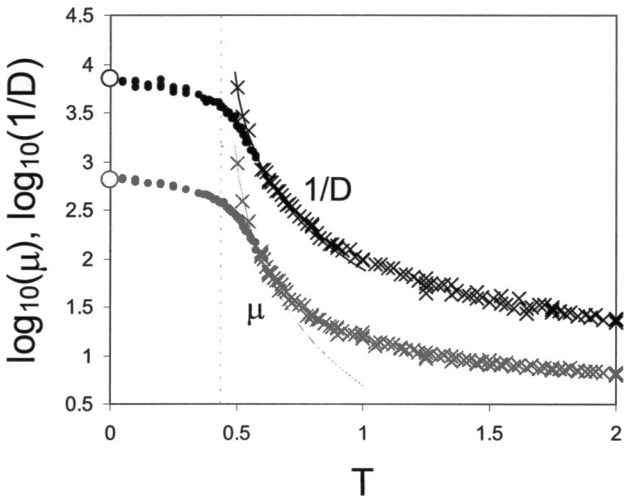

FIG. 1. Viscosity and inverse diffusivity as a function of temperature. The finite temperature results are from NEMD simulations, and the zero-temperature results (large open circles) are from the athermal simulations. Small filled circles, $\gamma=0.001$; crosses, $\gamma\to 0$; solid lines, $\mu\sim(T-T_c)^{-2.45}$ and $1/D\sim(T-T_c)^{-2.00}$, where $T_c=0.435$. The dashed line indicates the location of T_c.

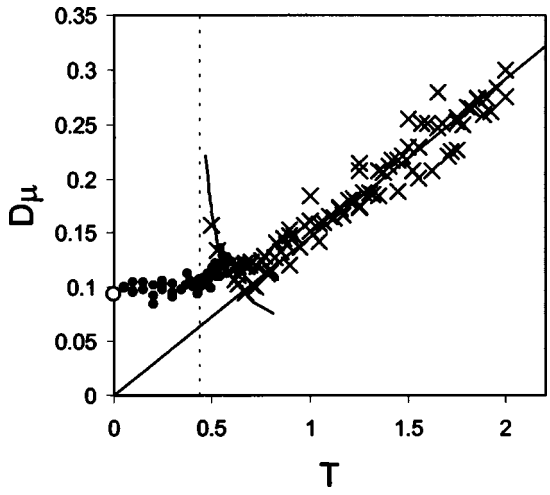

FIG. 2. The product of the viscosity and diffusivity as a function of temperature. The finite temperature results are from NEMD simulations, and the zero-temperature result (large open circle) is from the athermal simulations. Small filled circles, $\gamma=0.001$; crosses, $\gamma\to 0$; solid line, $D\mu\sim(T-T_c)^{-0.45}$, where $T_c=0.435$; diagonal line, Stokes-Einstein relation with $C_{\mathrm{SE}}=0.146$. The dashed line indicates the location of T_c.

The divergences of μ and $1/D$ at low temperature are avoided at the shear rate $\gamma=0.001$. The viscosities at $\gamma=0.001$ are smaller than the $\gamma\to 0$ values, and this "shear thinning" has been found in experiments on colloidal systems [6] and simulations of atomic systems [7]. The diffusivities at $\gamma=0.001$ are greater than the $\gamma\to 0$ values, and this shear-enhanced diffusion has also been found in experiments on colloidal systems [8] and simulations of atomic systems [9,10]. The temperature dependence of the viscosity and diffusivity at $\gamma=0.001$ becomes much weaker for $T<T_c$, and these properties extrapolate to finite values as $T\to 0$.

The product of the viscosity and diffusivity is shown as a function of T in Fig. 2. When the Stokes-Einstein relation is followed,

$$D\mu=TC_{\mathrm{SE}}, \tag{4}$$

where C_{SE} is a constant. The Stokes-Einstein relation is followed at higher temperatures, and the value of the constant $C_{\mathrm{SE}}=0.146$ is found by fitting to the high-temperature results ($T>1$). The Stokes-Einstein relation breaks down at lower temperatures for both the $\gamma\to 0$ and finite γ results, but the nature of the Stokes-Einstein breakdown is very different in these two cases.

For the $\gamma\to 0$ results, the product $D\mu$ diverges as the mode coupling temperature T_c is approached. Since $\mu\sim(T-T_c)^{-2.45}$ and $D\sim(T-T_c)^{2.00}$ for this system [3,5], the product $D\mu\sim(T-T_c)^{-0.45}$, which diverges as T approaches T_c. This divergence is in accord with results of previous simulations [11,12,13] and experiments [14,15], which find that the product $D\mu$ becomes much larger than the Stokes-Einstein value as a liquid becomes highly supercooled. This large increase in $D\mu$ has been attributed to heterogeneous dynamics in strongly supercooled liquids [11,15,16,17], where the size of the mobile regions diverges as T approaches T_c [18,19].

In contrast, at finite γ, the product $D\mu$ levels off to a finite value, rather than diverging. For low temperatures, the product $D\mu$ is equal to a constant (to within the errors of the simulation). Thus a different Stokes-Einstein-like relation appears to apply to sheared systems at low temperature,

$$D\mu=C_{\mathrm{ASE}}, \tag{5}$$

where C_{ASE} is the constant in this athermal-Stokes-Einstein-like relation; the value of $C_{\mathrm{ASE}}=0.0983$ (obtained from an average of the NEMD results for $T<0.35$).

The origins of this athermal-Stokes-Einstein-like relation become clear from the athermal simulations. As shown in Fig. 3, the shear stress usually increases continuously with strain, but these changes are punctuated by discontinuous drops. Also, the mean-squared displacement (relative to the positions at an initial configuration) usually varies little with strain, but undergoes occasional discontinuous jumps at the same points as the discontinuous stress drops. We have shown previously that these discontinuous changes follow strain-activated relaxations that occur when strain causes a local energy minimum to flatten out until it disappears [20,21,22,23], as shown schematically in Fig. 4 [24]. These strain-activated relaxations reduce stress and lead to atomic displacements.

The viscosity and diffusivity in the limit of zero temperature can be obtained from averaged results of the athermal simulations, shown in Figs. 3(c) and 3(d). The average shear stress is a constant value $C_\mu=0.649$ (after an initial transient period; the fluctuations are due to the relatively small num-

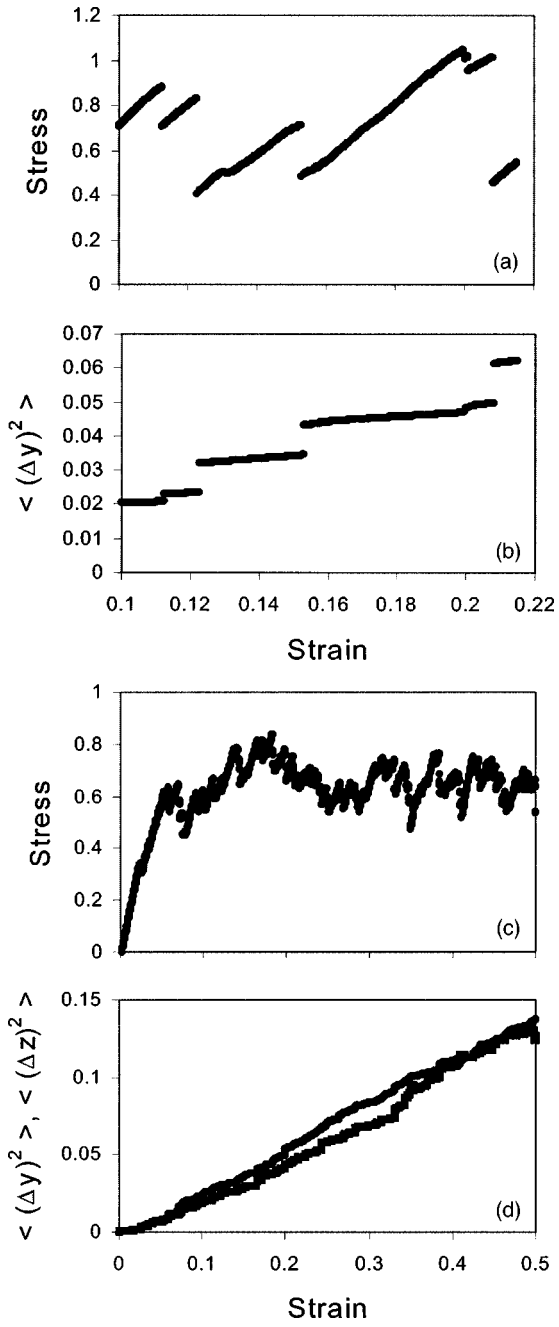

FIG. 3. Results from athermal simulations. (a) Shear stress and (b) mean-squared displacement for a single run. (c) Shear stress and (d) mean-squared displacement for an average of ten runs.

ber of samples used for the averaging), and so the viscosity $\mu = C_\mu/\gamma$ [see Eq. (1)] [23]. The mean-squared displacements in the directions perpendicular to flow increase linearly with strain (again, after an initial transient period), with the slope $2C_D = (\langle y^2\rangle/\lambda + \langle z^2\rangle/\lambda)/2 = 0.285$; the Einstein equations [Eq. (3)] can be multiplied and divided by the strain rate to yield

$$D_{yy} = \left(\frac{1}{2}\frac{\langle(\Delta y)^2\rangle}{\lambda}\right)\gamma, \quad D_{zz} = \left(\frac{1}{2}\frac{\langle(\Delta z)^2\rangle}{\lambda}\right)\gamma \qquad (6)$$

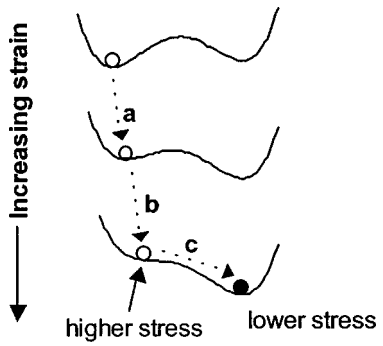

FIG. 4. Schematic representation of a strain-induced disappearance of an energy minimum. The curves represent the potential energy along the relevant coordinate, and the circles represent the state of the system. The change in the state of the system denoted by arrow "*c*" corresponds to a strain-activated relaxation process.

(note $\lambda = \gamma t$) and so the average diffusivity $D = C_D\gamma$ [20]. The athermal results for the viscosity and diffusivity are in excellent agreement with the extrapolation of the NEMD results to zero temperature, as shown in Fig. 1.

The product $D\mu$ under athermal shear flow can be evaluated as $D\mu = [C_D\gamma][C_\mu/\gamma] = C_D C_\mu$. Thus the athermal simulations yield $D\mu = C_{\rm ASE}$, as found empirically in our NEMD simulations. The constant $C_{\rm ASE} = C_\mu C_D = 0.0924$ from the athermal simulations, which agrees well with the NEMD result $C_{\rm ASE} = 0.0983$ (see also Fig. 2).

The product $D\mu$ can be used to define an effective temperature, $T_{\rm eff}^{\rm SE} = D\mu/C_{\rm SE}$ [25]; when the Stokes-Einstein relation is followed, $T_{\rm eff}^{\rm SE} = T$. At finite shear rate and low temperatures ($T < \sim 0.35$), $T_{\rm eff}^{\rm SE}$ has the constant value $T_{\rm eff}^{\rm SE} \approx 0.65$ ($T_{\rm eff}^{\rm SE} = 0.67$ is obtained from an average of the NEMD results for $T < 0.35$, and $T_{\rm eff}^{\rm SE} = 0.63$ is obtained from the athermal simulations). Thus $T_{\rm eff}^{\rm SE}$ gives a similar value at $T = 0.3$ and $\gamma = 0.001$ to an effective temperature based on fluctuation-dissipation theory ($T_{\rm eff}^{\rm FD}$), for which $T_{\rm eff}^{\rm FD} = 0.65$ at $T = 0.3$ and $\gamma = 0.001$ [5].

The viscosity increases as the driving force (shear stress) is decreased in athermal systems, and as temperature is decreased in thermal systems at $\gamma \to 0$; when the viscosity becomes so high such that flow does not occur on the time scales of the experiment, a jamming transition occurs. The present results show that the behavior of $D\mu$ is very different as jamming is approached by cooling as opposed to reducing the driving force: $D\mu$ diverges as jamming is approached upon cooling, but $D\mu$ maintains a finite value as jamming is approached by reducing the driving force. Since the divergence of $D\mu$ has been attributed to dynamic heterogeneities [11,15,16] the present results suggest that while dynamic heterogeneties are important as jamming is approached by cooling, the dynamic heterogeneities play a different role as jamming is approached by reducing the driving force (i.e., in shear-induced dynamics).

Funding for this project was provided by the NSF (Grant No. DMR-0080191).

[1] A. J. Liu and S. R. Nagel, Nature (London) **396**, 21 (1998).
[2] F. H. Stillinger and T. A. Weber, Science **225**, 983 (1984); F. H. Stillinger, *ibid.* **267**, 1935 (1995).
[3] W. Kob and H. C. Andersen, Phys. Rev. Lett. **73**, 1376 (1994).
[4] D. J. Evans and G. P. Morriss, *Statistical Mechanics of Nonequilibrium Liquids* (Academic Press, London, 1990).
[5] L. Berthier and J.-L. Barrat, J. Chem. Phys. **116**, 6228 (2002).
[6] W. B. Russel, D. A. Saville, and W. R. Schowalter, *Colloidal Dispersions* (Cambridge University Press, Cambridge, 1989).
[7] D. J. Evans, Phys. Rev. A **23**, 1988 (1981).
[8] X. Qiu, H. D. Ou-Yang, D. J. Pine, and P. M. Chaikin, Phys. Rev. Lett. **61**, 2554 (1988).
[9] D. M. Heyes, J. J. Kim, C. J. Montrose, and T. A. Litovitz, J. Chem. Phys. **73**, 3987 (1980).
[10] P. T. Cummings, B. Y. Wang, D. J. Evans, and K. J. Fraser, J. Chem. Phys. **94**, 2149 (1991).
[11] R. Yamamoto and A. Onuki, Phys. Rev. Lett. **81**, 4915 (1998).
[12] C. DeMichele and D. Leporini, Phys. Rev. E **63**, 036701 (2001).
[13] D. N. Perera and P. Harrowell, Phys. Rev. Lett. **81**, 120 (1998).
[14] F. Fujara, B. Geil, H. Silescu, and G. Fleischer, Z. Phys. B: Condens. Matter **88**, 195 (1992).
[15] M. T. Cicerone and M. D. Ediger, J. Chem. Phys. **104**, 7210 (1996).
[16] F. A. Stillinger and F. A. Hodgdon, Phys. Rev. E **50**, 2064 (1994).
[17] S. C. Glotzer, V. N. Novikov, and T. B. Schroder, J. Chem. Phys. **112**, 509 (2000).
[18] W. Kob, C. Donati, S. J. Plimpton, P. H. Poole, and S. C. Glotzer, Phys. Rev. Lett. **79**, 2827 (1997); C. Donati, S. C. Glotzer, and P. H. Poole, *ibid.* **82**, 5064 (1999).
[19] J. Qian, R. Hentschke, and A. Heuer, J. Chem. Phys. **111**, 10 177 (1999).
[20] D. L. Malandro and D. J. Lacks, Phys. Rev. Lett. **81**, 5576 (1998).
[21] D. J. Lacks, Phys. Rev. Lett. **80**, 5385 (1998).
[22] D. L. Malandro and D. J. Lacks, J. Chem. Phys. **110**, 4593 (1999).
[23] D. J. Lacks, Phys. Rev. Lett. **87**, 225502 (2001).
[24] The present interatomic potential has a discontinuous force at the cutoff distance, which can also lead to discontinuous changes in the stress with strain. However, this aspect of the potential would not give rise to the discontinuous changes in the mean-squared displacement with strain shown in Fig. 3(a). Also, our previous work (Refs. [21] and [22]) used potentials in which the forces (and all derivatives of the energy) are continuous everywhere, and the discontinuous changes in properties with strain were also observed. Therefore, the discontinuous changes in properties with strain shown in Figs. 3(a) and 3(b) are real effects, and not artifacts of the interatomic potential.
[25] I. K. Ono, C. S. O'Hern, D. J. Durian, S. A. Langer, A. J. Liu, and S. R. Nagel, Phys. Rev. Lett. **89**, 095703 (2002).